Migration of constituent atoms and interface morphology in a heterojunction between CdS and $CuInSe_2$ single crystals

Y. L. Soo, S. Huang, and Y. H. Kao
Department of Physics, State University of New York at Buffalo, Amherst, New York, 14260

S. K. Deb and K. Ramanathan
National Renewable Energy Laboratory, 1617 Cole Blvd., Golden, Colorado 80401

T. Takizawa
Nihon University, Japan

(Received 27 May 1999; accepted for publication 20 August 1999)

Angular dependence of x-ray fluorescence (ADXRF), x-ray absorption fine structure (XAFS), and grazing incidence x-ray scattering measurements were carried out using synchrotron radiation for a study of the interface morphology and migration of constituent atoms in a heterojunction formed between CdS and $CuInSe_2$ single crystals. The advantage of using a single crystal for this study is to avoid the usually complicated problems arising from multiple phases of the Cu–In–Se compounds. By a comparison of the results obtained with a bare $CuInSe_2$ single crystal, the changes of interface microstructures in the CdS/$CuInSe_2$ heterojunction system with *well-defined stoichiometry* can therefore be investigated. Prominent features in the ADXRF data clearly demonstrate that both Cu and Se atoms have migrated into the CdS layer in the heterojunction while In atoms remain intact in the $CuInSe_2$ single crystal. The local structures around Cu in the system also show a significant change after the deposition of CdS, as manifested by the appearance of new Cd near neighbors in the XAFS spectra. © *1999 American Institute of Physics.* [S0021-8979(99)02223-9]

I. INTRODUCTION

The chalcopyrite systems $CuInSe_2$ (CIS) and $Cu(In,Ga)Se_2$ (CIGS) are promising photovoltaic (PV) materials for the development of high efficiency solar cells. A record efficiency of 18.8% has been achieved recently in a thin film device consisting of a CIGS absorber and CdS window.[1] However, these chalcopyrite compounds normally contain a high density of defects. Efforts to improve the PV efficiency are often hindered by the lack of a clear understanding of the detailed microscopic structure in thin films of these compounds. Problems concerning phase separation, interface morphology, and compositional nonuniformity still remain as a major challenge for optimizing the performance of PV devices with CIS and CIGS thin films.

Previous experimental studies of this chalcopyrite system have been mostly on polycrystalline thin films which usually contain regions of different phases. For example, in the CIS system, additional phases such as $CuIn_3Se_5$ and $CuIn_5Se_8$ (socalled 1–3–5 and 1–5–8 phases) could usually be found. The presence of multiphase components generally makes it difficult to identify the underlying phase responsible for the high efficiency sunlight conversion and also could lead to ambiguous interpretations of experimental data in microstructural studies. To date, the morphology of the interface between CdS and CIS in the important CdS/CIS heterojunction is still not clearly understood. It is well known that the interdiffusion of constituent elements across the heterointerface could give rise to significant compositional changes and therefore affect the physical properties of both CIS and CdS. The presence of multiphase components in CIS can further complicate these problems. For the purpose of clarifying the microstructure and morphology and to improve the film quality for advanced PV applications, systematic material characterization starting with a simpler system of bulk CIS and heterojunctions by using a well-defined CIS single crystal would seem very useful.

In the present work, microstructure and surface morphology of a single crystal CIS are investigated for the first time using hard x rays from synchrotron radiation. Techniques of angular dependence of x-ray fluorescence (ADXRF) extended x-ray absorption fine structure (EXAFS), near-edge x-ray absorption fine structure (NEXAFS), and grazing incidence x-ray scattering (GIXS) have been used. For a comparison of possible differences in microstructure and morphology between a single crystal CIS and a CIS/CdS heterojunction, a thin film of CdS was deposited on the CIS crystal to form a heterojunction and the composite sample was then subjected to the same x-ray investigation. Our results provide useful information on the changes in depth distribution of the constituent atoms, surface morphology, as well as the local structure around Cu and Se before and after the formation of the heterojunction.

II. EXPERIMENT

The single crystal material used in the present study was grown by the horizontal Bridgeman method described earlier.[2] In this method, the mixture of Cu+In and Se were sealed in a quartz tube under vacuum. The Cu+In mixture, separated from Se, was first heated to 700 °C to form a CuIn alloy in a two-temperature zone furnace. The CuIn alloy was then heated to 1020 °C in the high temperature zone and Se was heated in the low temperature zone to maintain the de-

sired Se pressure. Selenium then reacted with the CuIn alloy to form a $CuInSe_2$ single crystal in the high temperature zone. The surface of this single crystal was a (112) plane, on which a CdS thin layer was later deposited to form a CdS/CIS heterojunction.

The CdS thin film on CIS was grown by chemical bath deposition. The bath was constituted by mixing 0.0015 M $CdSO_4$, 1.5 M NH_4OH, and 0.15 M thiourea at room temperature. The CIS crystal was suspended in the solution, and the temperature of the solution was ramped from room temperature to 70 °C in about 5 min. During this time, the CdS thin film of 40–50 nm thickness was deposited on the CIS crystal. This procedure allows a heterogeneous growth of the CdS film, and colloidal formation is minimized. The samples were rinsed in high purity deionized water, followed by a thorough ultrasonic rinse. No heat treatment of the sample was given.

An ADXRF technique was employed to investigate the depth distribution of Cu, Se, and In in the pure $CuInSe_2$ single crystal and in the CdS-coated heterojunction sample. By a comparison, these results allow us to probe possible migration of the constituent atoms from the $CuInSe_2$ single crystal to the CdS overlay. Since the $K\alpha$ radiation energies of these elements are well separated, this technique is element specific, thus making it possible to study changes in the depth distribution of Cu, Se, and In atoms separately.

In an ADXRF experiment, x-ray fluorescence pertaining to a selected element in the material under study is measured as a function of the x-ray penetration depth by varying the incidence angle of radiation. The angular dependence of the total fluorescence yield (FY) can be obtained from

$$I_{\mathrm{FY}} \propto \int dz \left(-\frac{dS_z(z)}{dz} \right) \Phi(z), \tag{1}$$

where S_z is the z component (perpendicular to the sample surface) of the Poynting vector, and $\Phi(z)$ is the density profile of the fluorescent atoms in the z direction,[3,4] from which information about the depth distribution of a specific element can be extracted. Detailed experimental procedures have been reported elsewhere.[5,6]

The generic features of the ADXRF output are illustrated with the results of a model calculation assuming uniform depth distribution of constituent atoms as shown in Fig. 1. Curve A represents the FY intensity as a function of incident grazing angle θ for a specific element with constant depth profile $\Phi(z)$ in a multicomponent bulk solid (e.g., FY of Cu, Se, or In from a single crystal $CuInSe_2$). The gradual rise of the FY from $\theta=0$, and an abrupt jump, followed by a nearly flat very slow increase at high angles reflect the variation of x-ray flux with an increasing grazing angle in the bulk material.[7] Curve B shows the general angular dependence of the FY intensity of the same element as in curve A for a bulk solid but coated with a thin film containing different elements (e.g., Cu FY from a single crystal of $CuInSe_2$ with a coated film of CdS). Note that since the overlay does not contain the element whose FY is being measured, there is no FY output at very low angles until the incident x-ray beam reaches a critical angle (about 0.1° in the present case of 400 Å CdS coating on CIS to penetrate into the bulk solid (CIS)

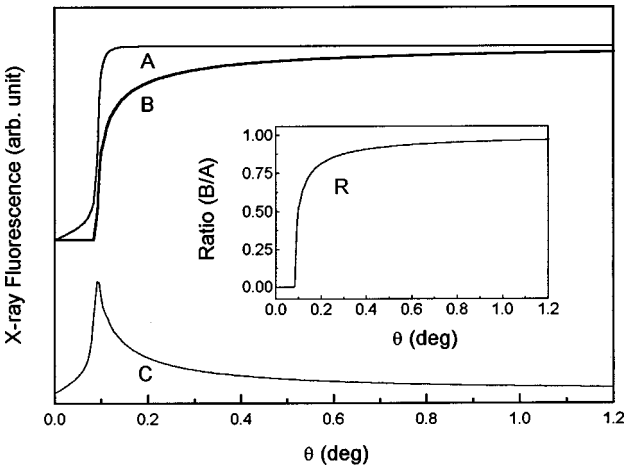

FIG. 1. Model calculation to illustrate the typical outputs of ADXRF measurements. Curve A: FY as a function of grazing incidence angle for an element in a bulk solid. Curve B: FY from the same element in the solid as curve A except that the bulk solid is coated with a thin film containing different elements. Curve C: FY due to an element in the overlay but not in the bulk solid. Curve R: ratio of curves B to A.

underneath the film. The rise of the FY after this critical angle is not as sharp as in curve A due to a redistribution of the photon flux in the composite system, and additional absorption has taken place in the coated layer for the incident and exit radiation. Curve C shows the general behavior of the FY from atoms in the overlay but not in the bulk solid underneath (e.g., Cd FY from a 400 Å CdS film coated on CIS), FY output starts at $\theta=0$ in the same way as in curve A, climbs up to a maximum around the critical angle, and then decreases to a low value at high angles. The presence of this maximum and the subsequent decrease are typical features of the FY from a thin film coating on bulk solid. The decrease of the FY after the maximum is mainly caused by lowered incident x-ray flux inside the film (with finite thickness) as the grazing angle is increased. Curve R in the inset shows the ratio of curve B to curve A, this ratio is more convenient for comparison with experimental data to avoid some complications due to geometrical factors.

In the present experiment, we have used an incident x-ray beam with photon energy of 28 keV to excite all the constituent elements in the samples under study. X-ray fluorescence photons from the irradiated samples were collected by using a Si(Li) detector calibrated with an energy resolution of 175 eV at the energy of Mn $K\alpha$ emission (5.899 keV). The $K\alpha$ fluorescence arising from each type of the constituent atoms were separated from other contributions by using a single-channel pulse-height analyzer and the FY results are plotted as a function of the grazing incidence angle θ between the incident x-ray beam and the film surface. The raw ADXRF data obtained from our CIS crystal and CdS/CIS junction are shown in Figs. 2(a) and 2(b), respectively. The FY output from Cd atoms in the CdS layer is also included in Fig. 2(b). The ratios of the ADXRF intensity of CdS/CIS to that of the single crystal CIS for each of the three elements Cu, Se, and In are shown in Fig. 2(c).

We have also measured Cu and Se K-edge EXAFS and NEXAFS using a standard fluorescence mode detection at room temperature to investigate the local structures around

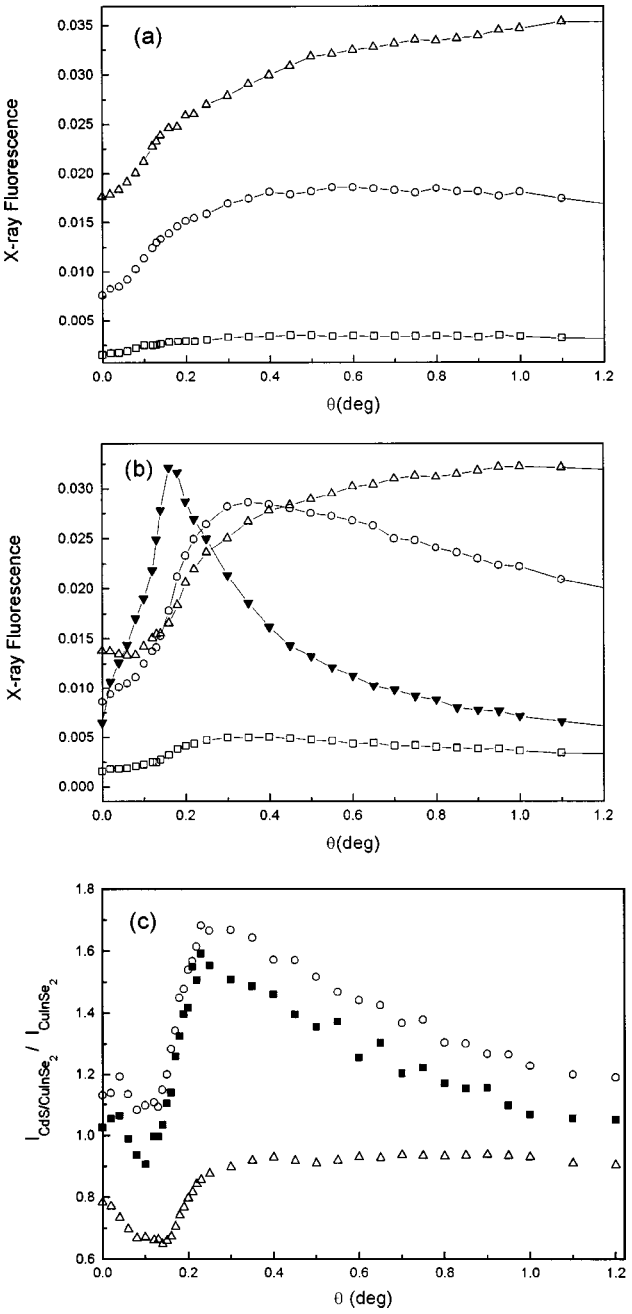

FIG. 2. (a) ADXRF raw data of different elements: In (triangles), Se (circles), and Cu (squares) in bulk $CuInSe_2$ single crystal. (b) ADXRF raw data of different elements: In (triangles), Se (circles), Cu (squares), and Cd (inverted solid triangles) in the $CdS/CuInSe_2$ heterojunction. (c) Ratio of ADXRF data of $CdS/CuInSe_2$ to that of bulk $CuInSe_2$ for In (triangles), Se (circles), and Cu (squares).

Cu and Se atoms and their effective valency in both samples. Detailed discussion of these absorption techniques can be found in several recent papers and review articles.[8–11] A well-established background-subtraction and correction method was used to extract the EXAFS χ functions from the raw experimental data.[8,9] The χ functions were then weighted with k or k^3 and Fourier transformed into real space for detailed comparison.[10,11] For a quantitative analysis of the local structures, the experimental data were analyzed and compared with theoretical calculations by a curve fitting method.[8,10,11] The χ functions and the corresponding Fourier transforms for Cu and Se *K*-edge EXAFS are shown in Fig. 3. These experimental curves are fitted with theoretical calculations using the coordination number and interatomic distances for $CuInSe_2$ derived from the x-ray diffraction data edited by Wyckoff.[12] By a comparison of theoretical calculations (heavy lines in Fig. 3) and the data (fine lines), parameters pertaining to the local environment surrounding Cu and Se atoms in CIS and in CdS/CIS heterojunction are obtained, as listed in Tables I and II. The Cu and Se *K*-edge NEXAFS results obtained with both CIS and CdS/CIS samples are plotted in Fig. 4 along with that of pure Cu and two model compounds of different valencies for comparison.

In addition, GIXS measurements were made to probe the interface morphology of the CdS/CIS heterojunction for a comparison of the surface roughness of the CIS single crystal before CdS deposition. The experimental setup and procedures, as well as details of data analysis, have been reported elsewhere.[12–16] Through a control of the x-ray probing depth and field distribution by varying the incidence angle, GIXS measurements allow a *nondestructive* method to obtain important microstructural information about the interfaces, such as the layer thickness, interfacial roughness, and correlation lengths of interface height fluctuations. For a multilayer structure, the specular reflection (with photon momentum transfer q_z perpendicular to the interface) can usually be treated by a matrix formulation using the Fresnel law of classical optics. To account for the interfacial roughness, the Fresnel law can be modified by introducing a rms height fluctuation (or roughness) parameter σ in a vector scattering model.[17] When the incidence angle is sufficiently far away from the critical angle, the scattering intensity is weak and Born approximation or a distorted-wave Born approximation[15,16] can be applied to investigate the effects of diffuse scattering, and the intensity can be calculated by introducing a correlation function between height fluctuations on different interfaces i and j of the following form

$$C_{ij}(x,y) = \langle \delta z_i(0,0)\, \delta z_j(x,y) \rangle = C_0(R) \exp[-|z_i - z_j|/\xi_\perp], \quad (2)$$

where $\delta z_i(x,y)$ is the height fluctuation on the ith interface at any point (x,y) a distance $R(x,y)=(x^2+y^2)^{1/2}$ from an arbitrary origin. $C_0(R)$ is the lateral (in-plane) correlation function which, in a simple model for statistical treatment of the random interfaces, can be expressed as $\sigma_i \sigma_j \exp[-(R/\xi_\parallel)^{2h}]$, where σ_i and σ_j are the rms roughness on the ith and jth interfaces, $\xi_\parallel$ and $\xi_\perp$ are the lateral- and cross-correlation lengths of interfacial height fluctuations in the layered structure, respectively; h is called a texture coefficient.[16] By a comparison of the x-ray diffuse scattering data with model calculations, the parameters σ's, $\xi_\parallel$, $\xi_\perp$, h and the layer thickness can be determined. More details of this method and theoretical background can be found in Refs. 15 and 16.

All the ADXRF, EXAFS, NEXAFS, and GIXS experiments were performed at beamline X3B1 at National Synchrotron Light Source at Brookhaven National Laboratory.

III. RESULTS AND DISCUSSION

The raw ADXRF curves for bulk $CuInSe_2$ are shown in Fig. 2(a) and those for the $CdS/CuInSe_2$ junction are shown in Fig. 2(b). In Fig. 2(a), all plots for the three elements in CIS resemble the general features demonstrated in Fig. 1 (curve A). The intensity difference between In, Se, and Cu is due to different cross sections in the generation of fluorescence (there is a large dependence on the atomic number Z). The general shape of In $K\alpha$ fluorescence of the CdS-coated CIS is similar to that of the bulk CIS except for a minor intensity decrease (~90% of the bulk CIS value) and a rise starts at an angle ~0.08°. The decreased overall FY intensity is mainly due to attenuation of In $K\alpha$ fluorescence in the CdS coated layer. The onset of the In FY at ~0.08° is caused by a larger depth through which the incident x-ray beam has to penetrate in order to reach the In atoms in the buried $CuInSe_2$ single crystal (as demonstrated in Fig. 1, curve B). These features are all as expected for a junction with a sharp interface (for the In atoms) and with a constant In concentration profile in CIS. The ratio of the In FY in the CdS/CIS junction to that in the CIS crystal is shown in Fig. 2(c). The initial decrease of this ratio below 0.1° is due to an edge effect (FY arising from In atoms when the incident x-ray beam is on the sample edge) and should be discarded. The overall angular dependence of this ratio can be compared with the general behavior demonstrated in our model calculation (curve R, Fig. 1).

In contrast to the characteristics of constant profile for In atoms, the results of the Cu and Se $K\alpha$ fluorescence show considerable changes after the CIS crystal is coated with a

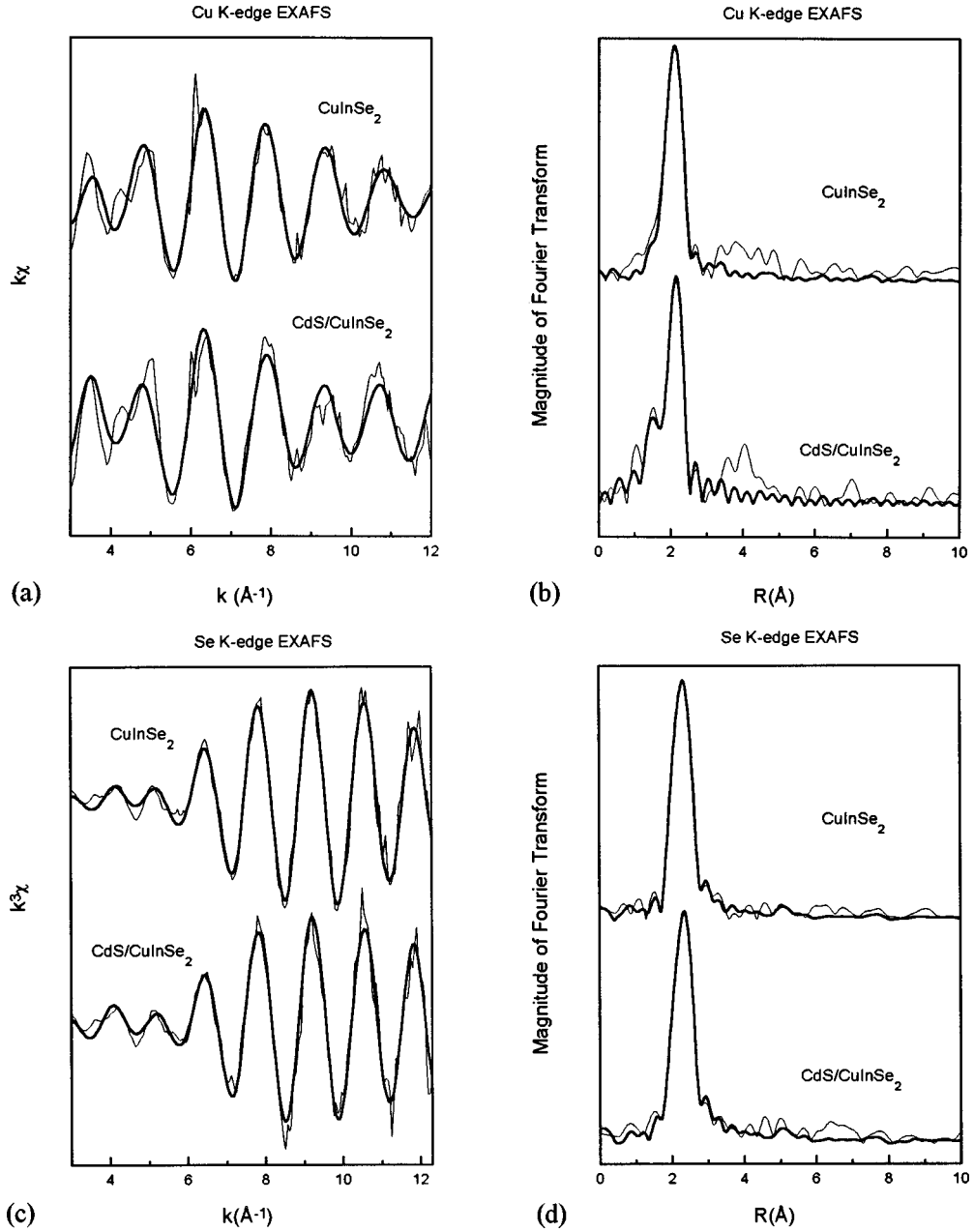

FIG. 3. (a) Weighted Cu K-edge EXAFS χ functions. (b) Fourier transform of Cu K-edge EXAFS χ functions. (c) Weighted Se K-edge EXAFS χ functions. (d) Fourier transform of Se K-edge EXAFS χ functions.

TABLE I. Local structures around Cu obtained from Cu *K*-edge EXAFS curve fitting. Underlined values were kept constant during fitting. *N* is the coordination number; *R* is the distance between the central (Cu) atom and neighboring atomic shells; σ^2 is a Debye–Waller factor serving as a measure of the local disorder. Values of *N* and Cu–Se interatomic distance for single crystal $CuInSe_2$ are calculated from x-ray diffraction data edited by Wyckoff.[a]

Sample	Atom	*N*	*R* (Å)	σ^2 (10^{-3} Å^2)	ΔE_0 (eV)	λ (Å)	S_0^2
$CuInSe_2$	Se	4	2.40	7	0.2		0.7
$CdS/CuInSe_2$	Cd	0.6	2.07	0.7	−6	6	0.7
	Se	4.3	2.38	5	−6		

[a]See Ref. 12.

CdS layer. The gradual decrease of the Cu and Se FY at high angles is indicative of a concentration gradient, resulting from a redistribution of these atoms. These curves are qualitatively similar to that of Cd in the CdS layer (a characteristic of higher concentration of Cd atoms near the sample surface), as also demonstrated in Fig. 1 (curve C) for a thin film overlay.

The ratio of the Cu and Se FY in the CdS/CIS junction to that in CIS is also shown in Fig. 2(c). All the variations below 0.1° in this plot should be discarded because of the complications of an edge effect noted before. At a low angle around 0.1°, the ratio is very close to unity (0.95 and 1.1 for Cu and Se, respectively) indicating that the concentration of Cu and Se near the junction surface is similar to that in the bulk $CuInSe_2$ sample, a clear indication of substantial migration of Cu and Se atoms from buried CIS to the CdS overlay. The FY of Cu and Se has increased to about 1.6–1.7 times above the respective bulk $CuInSe_2$ values at $\theta \sim 0.25°$. This increase of the Cu and Se $K\alpha$ FY, as well as the gradual decrease at higher angles, indicates that there are relatively higher concentrations of Cu and Se atoms located near the CdS/CIS junction sample top surface than in pure CIS.

Possible changes of local environment around Cu and Se as a result of CdS coating on CIS have been studied by using the Cu and Se *K*-edge EXAFS. The EXAFS χ functions and the corresponding Fourier transforms (similar to a pair distribution function except for some phase-related corrections) obtained with the CIS and CdS/CIS junction are shown in Fig. 3 for comparison. These data generally suggest that the local structures around Cu and Se in the CdS/CIS junction

TABLE II. Local structures around Se obtained from Se *K*-edge EXAFS curve fitting. Underlined values were kept constant during fitting. *N* is the coordination number; *R* is the distance between the central (Se) atom and neighboring atomic shells; σ^2 is a Debye–Waller factor serving as a measure of the local disorder. Values of *N* and Se–Cu interatomic distance for single crystal $CuInSe_2$ are calculated from x-ray diffraction data edited by Wyckoff.[a]

Sample	Atom	*N*	*R* (Å)	σ^2 (10^{-3} Å^2)	ΔE_0 (eV)	λ (Å)	S_0^2
$CuInSe_2$	Cu	2	2.40	0.9	6	11	0.5
	In	2	2.61	0.2	7		
$CdS/CuInSe_2$	Cu	1.4	2.36	0.2	−4	11	0.5
	In	2.3	2.59	0.2	4		

[a]See Ref. 12.

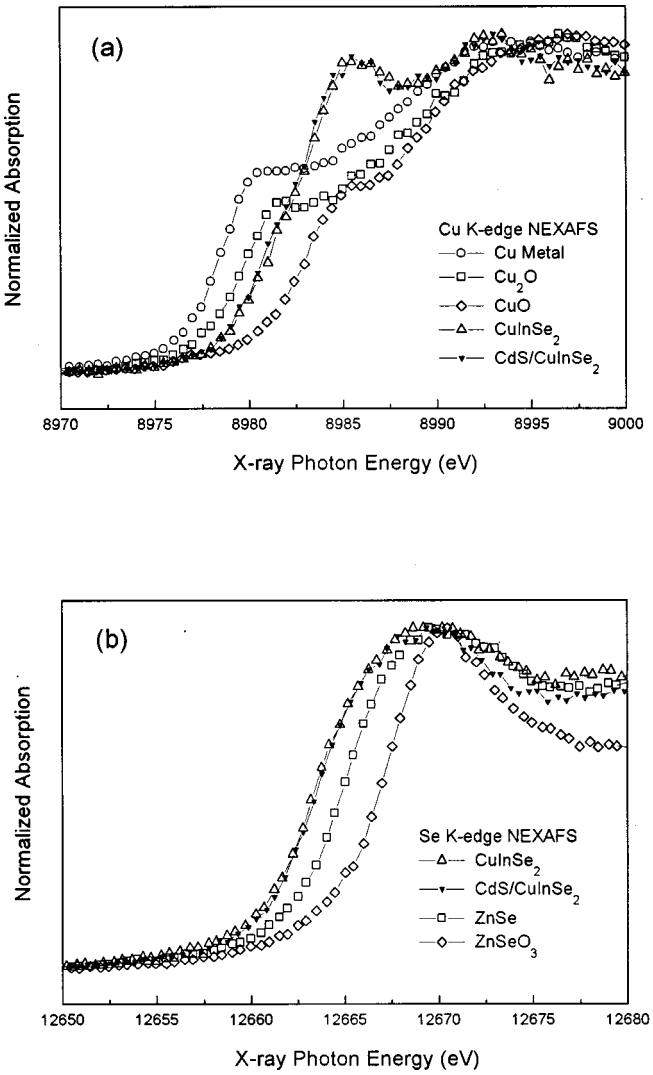

FIG. 4. (a) Cu *K*-edge NEXAFS for $CdS/CuInSe_2$, bulk $CuInSe_2$, pure Cu, and two model compounds. (b) Se *K*-edge NEXAFS for $CdS/CuInSe_2$, bulk $CuInSe_2$ and two model compounds.

are similar to those in the CIS single crystal. Results of detailed EXAFS analysis by curve fitting are presented in Tables I and II.

The prominent main peak in the Fourier transform of Cu χ functions [centered at ~2 Å in Fig. 3(b)] is due to the first-neighbor shell of Se atoms at a distance 2.40 Å from the Cu site in the chalcopyrite structure of $CuInSe_2$.[12] Within the accuracy of these measurements (about 2% uncertainty for the interatomic distances and 20% uncertainty for the coordination numbers), the shell of Se atoms surrounding Cu in the CdS/CIS junction remains practically the same as in CIS. However, the Fourier transform for the CdS/CIS junction contains an additional small peak to the left of the main peak [Fig. 3(b)]. As shown in Table I, this additional small peak is identified to be a new Cd neighbor shell around Cu with an average coordination number of 0.6 at a distance of 2.07 Å from the Cu atom. The appearance of Cd near neighbors around Cu is also consistent with our ADXRF observation that Cu atoms have migrated from CIS into the CdS layer in the CdS/CIS junction and possibly form some Cu–Cd complexes therein. It is equally possible, however,

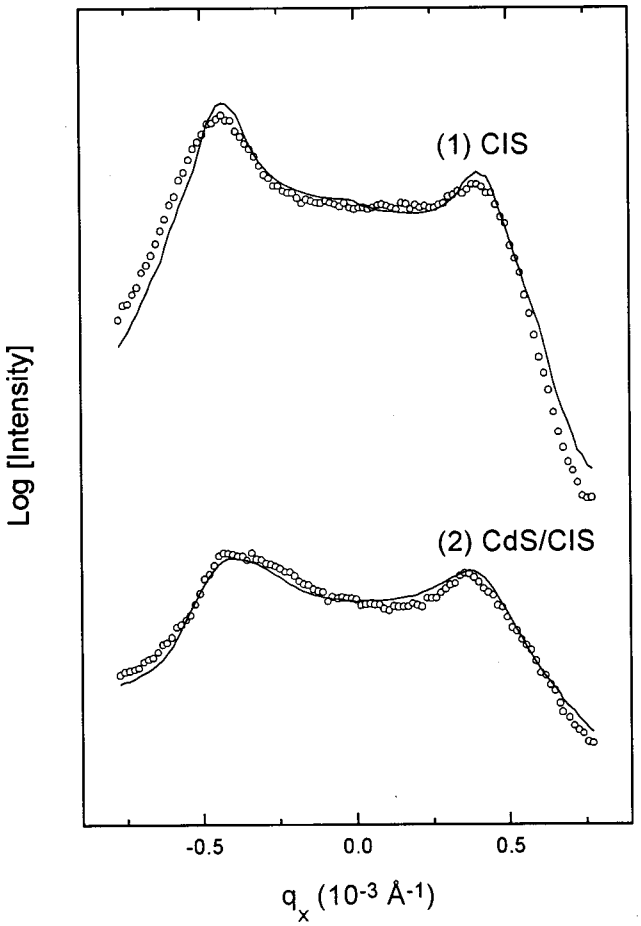

FIG. 5. TDS data (circles) for CIS and CdS/CIS heterojunction in comparison with theoretical calculations (lines).

that Cd atoms have diffused into CIS and show up as new neighbors around Cu.

The Fourier transforms of the Se EXAFS χ functions for CIS and CdS/CIS are shown in Fig. 3(d). Although the distances of first and second neighbor shells (Cu and In) in the junction are practically the same as in bulk CIS, there is an observable decrease of the coordination number of Cu neighbors after the CdS/CIS junction is formed. Since the Se EXAFS data provide information on an average of all Cu near neighbors in the entire junction system, this lowered coordination number can therefore be interpreted as a result of migration of both Cu and Se from CIS into the CdS layer where the average number of Cu–Se bonds is lower than that in crystalline CIS. On the other hand, the second neighbor atoms (In) surrounding Se remain intact after formation of the junction, also consistent with the ADXRF experiment.

The threshold energy of x-ray absorption edge observed in a NEXAFS spectrum can often be used to estimate the effective valency of a selected constituent element in the sample.[8,11] As expected from simple effective charge arguments, the edge shifts to a higher energy as the valency of the selected element increases. By a comparison with the NEXAFS spectra of some model compounds with known valencies as references, limits of *effective* valency of Cu and Se atoms in both the CIS and CdS/CIS junction can therefore be studied. As shown in Fig. 4, the effective valency of Cu in both samples is between $+1$ and $+2$ and that of Se is below -2. The NEXAFS curves for the junction are almost identical to those of bulk $CuInSe_2$, indicating that the average electronic structures around Cu and Se are similar.

TABLE III. Surface morphology parameters obtained from GIXS measurements. σ_0 is the rms surface roughness; h is the texture coefficient; $\xi_\parallel$ is the lateral-correlation length.

Sample	σ_0(Å)	h	$\xi_\parallel$(Å)
CIS	66±35	0.4±0.1	197±60
CdS/CIS	10±8	0.95±0.2	170±85

Figure 5 shows the data of transverse diffuse scattering (TDS) obtained in our GIXS experiment. The solid lines are theoretical calculations based on Eq. (2). From the theoretical fits, the surface roughness of the CIS and CdS/CIS junction samples can be obtained. This result is presented in Table III. It should be noted that the surface roughness of CIS is rather high. The texture coefficient h indicates that the surface height fluctuations are close to an exponential distribution, also suggesting a jagged surface. The surface of the CdS/CIS junction, on the other hand, is quite smooth and the height fluctuations are essentially Gaussian with h nearly equal to unity. The lateral correlation lengths are comparable for the two samples. Reflectivity and longitudinal diffuse scattering measurements were also made; all these data are dominated by diffuse scattering and no usual oscillations can be found.

It perhaps should be noted that the x-ray fluorescence, absorption, and scattering measurements using hard x rays can provide us with direct element-specific information on microstructures and interface morphology practically independent of the surface condition of the solids, hence, these techniques can be utilized for nondestructive characterization of the depth profile of selected atomic species in systems consisting of thin layers with large interfacial roughness. The probing depth of these techniques is over a micron, and there is no need to vary the sample thickness in order to study the depth profile. On the other hand, x-ray emission and photoelectron spectroscopy (XES/PES) measurements are very sensitive to surface contamination and the probing depth is limited by the short electron mean free path. Samples with different thickness smaller than the electron mean free path but larger than the interfacial roughness are needed. This requirement makes it difficult to study thin film systems with interfacial roughness comparable to the film thickness. For layer structures with large interfacial roughness and significant intermixing of constituent atoms in a depth larger than the electron mean free path, such as the heterojunctions between CdS and CIS (or CIGS), the results obtained from XES and PES spectra[18,19] could be severely affected by the large fluctuations in the interfacial roughness as well as variations in structural or chemical defects in the thin films of different thickness. A conclusion on In migration from CIGS into CdS derived from these surface-sensitive experiments[19] should perhaps be reconfirmed by further careful investigations.

IV. CONCLUSION

ADXRF, XAFS, and GIXS experiments have been carried out to investigate the intermixing of constituent atoms, microstructures, and interface morphology in a CdS/CIS heterojunction. To avoid the complication arising from multiple phases in the CIS system, a single crystal of CIS prepared by the Bridgeman method has been used. The fluorescence, absorption, and scattering measurements using hard x rays from synchrotron radiation are insensitive to the surface contamination and well suited for studying the density profile and interface morphology of buried thin films with large interfacial roughness.

By a direct comparison of experimental data obtained with a CIS single crystal and a CdS/CIS heterojunction, our results show that both Se and Cu can migrate from CIS into CdS while In remains intact within CIS.

ACKNOWLEDGMENTS

The present research is supported by DOE and NREL.

[1] K. Ramanathan *et al.* (unpublished).
[2] H. Matsushita and T. Takizawa, J. Cryst. Growth **160**, 71 (1996).
[3] A. Krol, C. Sher, and Y. H. Kao, Phys. Rev. B **38**, 8579 (1988).
[4] D. K. G. de Boer, Phys. Rev. B **44**, 498 (1991).
[5] Y. L. Soo, S. Huang, Y. H. Kao, and A. D. Compaan, J. Appl. Phys. **83**, 4173 (1998).
[6] Y. L. Soo, S. Huang, Y. H. Kao, and A. D. Compaan, Appl. Phys. Lett. **74**, 218 (1999).
[7] Z. H. Ming, A. Krol, Y. L. Soo, Y. H. Kao, J. S. Park, and K. L. Wang, Phys. Rev. B **47**, 16373 (1993).
[8] Y. L. Soo, Z. H. Ming, S. W. Huang, Y. H. Kao, R. N. Bhargava, and D. Gallagher, Phys. Rev. B **50**, 7602 (1994), and references cited therein.
[9] M. Newville, P. Lïvin, Y. Yacoby, J. J. Rehr, and E. A. Stern, Phys. Rev. B **47**, 14126 (1993).
[10] P. A. Lee, P. H. Citrin, P. Eisenberger, and B. M. Kincaid, Rev. Mod. Phys. **53**, 769 (1981).
[11] D. E. Sayers and B. A. Bunker, in *X-ray Absorption*, edited by D. C. Koningsberger and R. Prins (Wiley, New York, 1988), p. 211.
[12] R. W. G. Wyckoff, *Crystal Structures* (Interscience Publisher Inc., New York, 1960).
[13] Z. H. Ming, S. Huang, Y. L. Soo, Y. H. Kao, T. Carns, and K. L. Wang, Appl. Phys. Lett. **67**, 629 (1995).
[14] S. Huang, Z. H. Ming, Y. L. Soo, Y. H. Kao, M. Tanaka, and H. Munekata, J. Appl. Phys. **79**, 1435 (1996).
[15] Z. H. Ming, A. Krol, Y. L. Soo, Y. H. Kao, J. S. Park, and K. L. Wang, Phys. Rev. B **47**, 16373 (1993).
[16] S. K. Sinha, E. B. Sirota, S. Garott, and H. B. Stanley, Phys. Rev. B **38**, 2297 (1988).
[17] B. Vidal and P. Vincent, Appl. Opt. **23**, 1794 (1984).
[18] T. Löher, W. Jaegermann, and C. Pettenkofer, J. Appl. Phys. **77**, 731 (1995).
[19] C. Heske *et al.* Appl. Phys. Lett. **74**, 1451 (1999).